SANDIA REPORT SAND83—1898 • Unlimited Release • UC—~~13~~ 25
Printed September 1983

Stress-Wave Experiments on Selected Crustal Rocks and Minerals

SAND--83-1898

DE84 001613

Dennis E. Grady

Prepared by
Sandia National Laboratories
Albuquerque, New Mexico 87185 and Livermore, California 94550
for the United States Department of Energy
under Contract DE-AC04-76DP00789

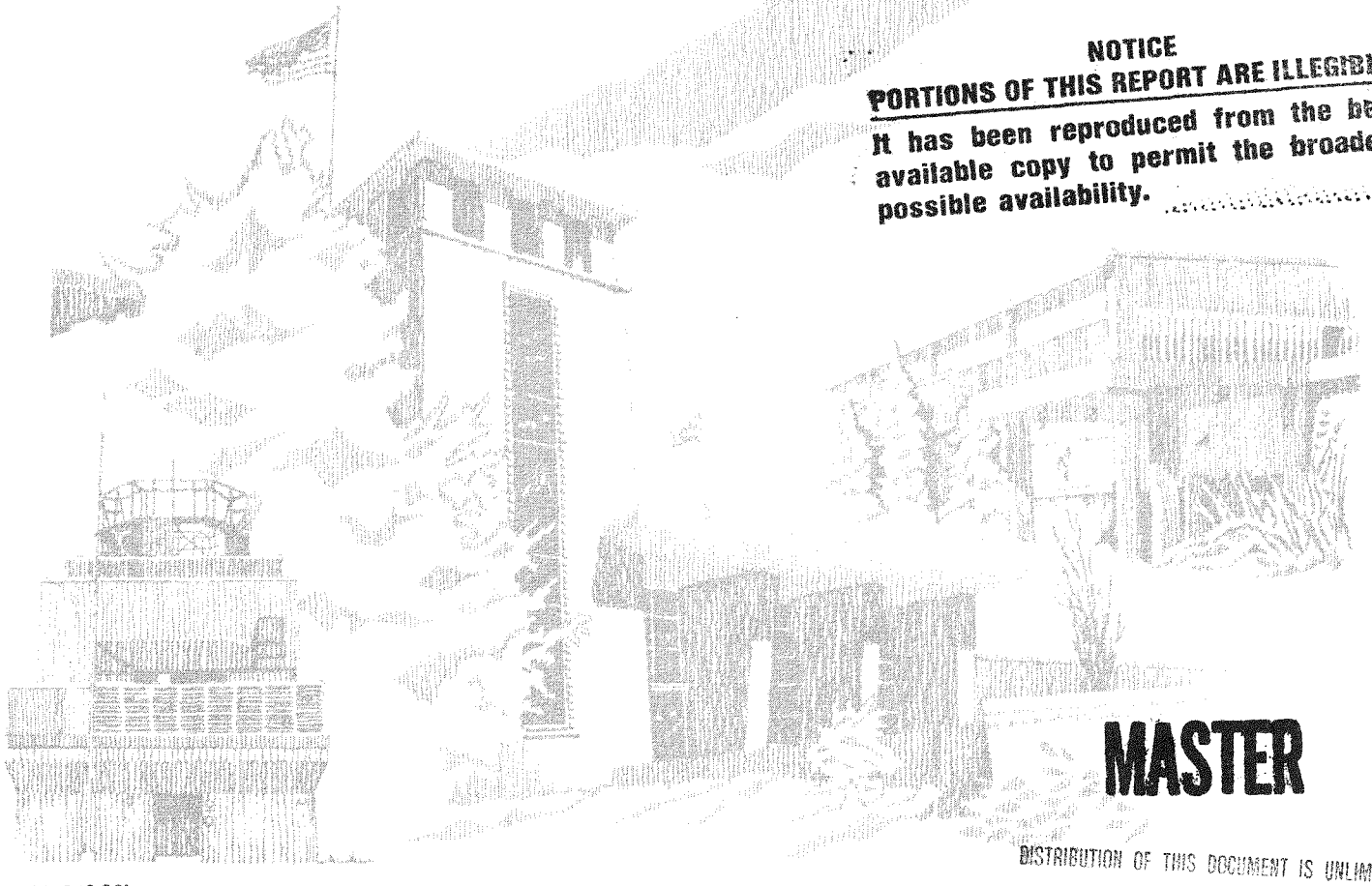

Issued by Sandia National Laboratories, operated for the United States Department of Energy by Sandia Corporation.

Printed in the United States of America
Available from
National Technical Information Service
U.S. Department of Commerce
5285 Port Royal Road
Springfield, VA 22161

NTIS price codes
Printed copy: A03
Microfiche copy: A01

Distribution
Category UC–13

SAND83-1898
Unlimited Release
Printed September 1983

Stress–Wave Experiments on Selected Crustal Rocks and Minerals

D. E. Grady
Thermomechanical & Physical Division, 1534
Sandia National Laboratories
Albuquerque, New Mexico 87185

ABSTRACT

Large-amplitude compressive stress-wave experiments on selected crustal rocks and minerals have been performed. The materials studied included Vermont marble, Blair dolomite, Oakhall limestone, z-cut calcite and oil shale. In each case specific constitutive features were studied. These features included interrelation of plastic yielding and phase transformation, rate dependent plastic flow, dilatancy under dynamic loading conditions, and energy dissipation at stress amplitudes below measured Hugoniot elastic limits. A new experimental method using in-material mutual-inductance magnetic gauges is also described.

DISCLAIMER

Contents

1 Introduction

Constitutive models capable of describing the dynamic deformation of geological materials are needed in a number of weapons and energy applications. The models are an integral part of the numerical code capability developed to support these programs. The deformation of crustal rocks can be complicated, as demonstrated by a large body of static triaxial studies. Features such as dilatancy, phase transformation, pressure dependent yielding, and fracture are observed and must be accounted for. Furthermore, when deformation is rapid due to impulsive loading, added complications of rate dependence and effective viscous behavior of the material may also play an important role. Assessment of these effects and their incorporation into current computational models are crucial to a modern calculational capability in this area.

The selected studies described in the present report were undertaken in response to uncertainties in the dynamic response of various rocks during the course of constitutive model development over the past few years. Each piece of work described here was relatively short and was concluded either when the crucial question had been answered or when it was recognized that a thorough study would be more extensive than near-term program needs warranted. In several cases results were actually negative. For instance static compression studies had indicated that dilatancy under uniaxial strain compression was an important effect in certain rocks. Stress-wave experiments performed in the present work showed that dilatancy was not occurring at the higher loading rates, and thus it is apparently sensitive to the rate of loading.

All compression wave experiments in this study were performed by normal planar impact studies with a 100 mm bore diameter light gas gun. Both Michelson and velocity interferometry provided the primary instrumentation although magnetic mutual inductance rings were used in one study to measure dynamic strain.

In the first set of experiments the dynamic uniaxial strain response of Vermont marble is determined from transmitted wave profile measurements. Vermont marble, a metamorphic rock, is found to yield by plastic flow prior to onset of the calcite I-II phase transition. This contrasts with earlier studies in limestone rock which indicated that transformation initiated within the elastic range and delayed plastic yielding until substantially larger axial stress levels were achieved.

In the next section special experiments on Blair dolomite are described which were performed to measure the rate of stress relaxation. Earlier experiments showed that, for uniaxial loading rates in excess of 10^4/s, dynamic response differed markedly from low rate response. In the present tests, effective loading strain rates near 10^3/s were achieved and stress relaxation was not observed.

Experiments were also performed on Oakhall limestone to evaluate effects of dilatancy under dynamic uniaxial-strain loading. Such effects have been observed in similar static tests. In addition to velocity interferometer measurements, time-resolved strain was monitored with a magnetic mutual inductive technique. In contrast to the static tests, dilatancy was not observed in the dynamic experiments.

In the following section exploratory experiments on single crystal (z-cut) calcite are described where loading through the shear sensitive calcite I-II transition is achieved. A complex wave structure involving both plastic flow and phase change is observed which differs markedly from the response of calcite rock.

Lastly, pulse-wave attenuation experiments on oil shale are presented. Peak stresses achieved are well below the measured Hugoniot elastic limit for this material; however, viscoelastic dissipation and/or geometric dispersion results in significant attenuation in terms of strain energy lost from the head of the pulse.

2 Compression Wave Studies of Vermont Marble

The experiments described here are the last of a study of the dynamic constitutive response of carbonate rocks. Earlier studies include Blair dolomite[1], Solenhofen limestone[2], and Oakhall limestone[3]. Vermont marble was selected as representative of coarse grained, metamorphosed calcite rock, to contrast with the earlier sedimentary rock types. Interpretation and analysis of these data have been previously published[4,5,6]. Documentation of the data here with the associated experimental conditions has been undertaken to provide verification for geological material models.

2.1 Experimental Method

The experimental methods used to investigate the wave propagation properties of Vermont marble under plate impact loading have been described in detail[1]. Only features unique to this set of tests will be discussed. Earlier studies on Solenhofen and Oakhall limestone[2,3] have been more extensive in that typically three tests with different sample thicknesses were performed at the same impact velocity to determine wave evolution characteristics. Four or five different impact velocities were then tested constituting 12 to 15 experiments. In the present series only one sample thickness was selected (with two exceptions) and only the impact velocity was varied. It was believed from the earlier studies on Solenhofen and Oakhall limestone that the wave evolution was reasonably well understood and we were primarily searching for differences in the wave propagation behavior.

The Vermont marble used in the present study has a density of 2710 kg/m^3 with a porosity of less than 0.5%. The grain size ranged from 0.2 to 1.0 mm. The measured ultrasonic longitudinal and shear wave velocities were 5.40 km/s and 2.89 km/s, respectively.

Velocity interferometer records were somewhat noisier than similar data obtained on dolomite[1] and limestone[2,3]. This was attributed to the larger grain size of the marble and the significant elastic anisotropy of the calcite grains. Two procedures were implemented to reduce the noise. First, a fused silica buffer was placed between the back surface of the marble and the recording interface in hopes of smoothing the wave prior to recording. Second, the laser beam was defocused to enlarge the area over which material velocity is measured.

Although some improvements were noted in the records, the efforts were not entirely satisfactory.

2.2 Experimental Results

The test conditions for the eight experiments on Vermont marble are provided in Table I and the measured velocity interferometer profiles are displayed in Figures 1 and 2. A composite display of VM 101 through VM 105 is shown in Figure 3.

The wave velocity corresponding to sample transit of the first wave arrival was determined on seven tests and showed a scatter of approximately 10%. This contrasts with the same measurements on dolomite and limestone where scatter of less than 2% was achieved. Again this is attributed to the large grain size ($\sim$ 0.5 mm) compared to the sample thickness of approximately 8 mm. The average velocity of 6.19 km/s is significantly larger than the longitudinal ultrasonic velocity.

Several distinct features are identified in the wave profiles in Figure 3. Two breaks are observed fairly close together in the initial rise of the wave and identified by 1 and 2 in Figure 3. These have been associated with plastic yielding and onset of the calcite I-II phase transformation, respectively[4]. A third break on loading (point 3) appears to correspond to onset of the second, calcite II-III, shock-induced phase transformation[4]. Points 4 and 5 on the release wave profile have been related to reversion of the sluggish calcite II-III and the displacive calcite I-II transition, respectively[4].

Table I
Compression Wave Experiments on Vermont Marble

Shot Number	Sample Thickness (mm)	Impactor* Thickness (mm)	Buffer† Plate (mm)	Projectile Velocity (km/s)	First Arrival Velocity (km/s)
VM101	7.951	4.764	0	0.321	6.01
VM102	7.949	4.773	0	0.659	–
VM103	7.958	4.756	0	0.496	6.20
VM104	7.950	4.737	3.243	0.410	6.22
VM105	7.945	4.764	3.135	0.577	6.52
VM106	7.970	4.732	3.218	0.650	5.91
VM107	14.993	6.022	3.245	0.519	6.08
VM108	9.415	5.020	3.255	0.527	6.40

*With the exception of VM 108 all impactors were fused silica backed by a void. In VM 108 a dead soft copper impactor was used.

†Buffer plate and window were fused silica on all experiments.

2.3 Discussion

The features observed in the Vermont marble wave profiles are quantitatively similar to the data measured on Oakhall and Solenhofen limestone with the exception of the initial yield behavior. This appears to be microstructure dependent. In Solenhofen and Oakhall limestone initial yielding occurred at a stress of 0.6 and 1.0 GPa, respectively, and is attributed to onset of the calcite I-II phase transition rather than plastic flow. In Vermont marble the wave structure indicates two breaks between 0.8 and 1.2 GPa. It appears that plastic yielding occurs first in Vermont marble and the second break corresponds to onset of phase transformation. As a consequence of this, the initial behavior of Vermont marble is strain rate sensitive in contrast to that of the two limestones studied. Comparison with static uniaxial and triaxial data support this observation[4,5].

The measured wave profiles are unsteady waves with a finite rise time and, strictly speaking, the peak stress states are not Hugoniot states. The difference is slight, however, and the approximate Hugoniot points for Vermont marble are compared with hydrostatic compression curves for calcite in Figure 4. Aragonite is the stable high-pressure phase above approximately 0.3 GPa; however, the metastable phases calcite II and then calcite III are achieved instead under static

compression. From the Vermont marble Hugoniot in Figure 4 it is clear that the calcite II and calcite III phases are also achieved under shock compression. The full volume change in the displacive calcite I-II transformation is quickly attained. The offset between the static and dynamic transition stress can be explained by shear-stress effects[6]. Complete transformation to the calcite III phase is not achieved until an overpressure of approximately twice the static transformation pressure is realized. The behavior is characteristic of shock-induced reconstructive transformations in silicate rocks.

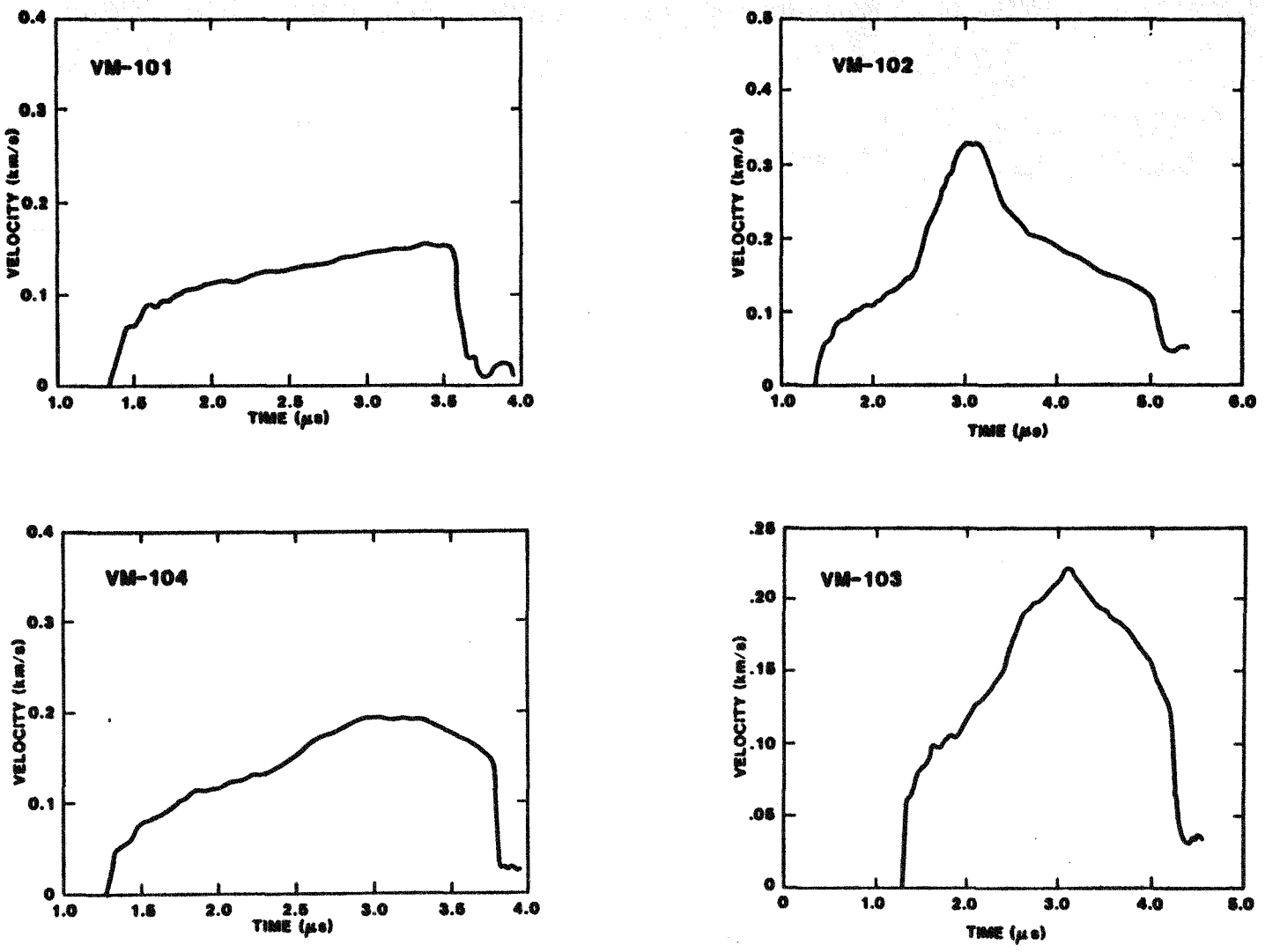

Figure 1. Particle velocity profiles in Vermont marble.

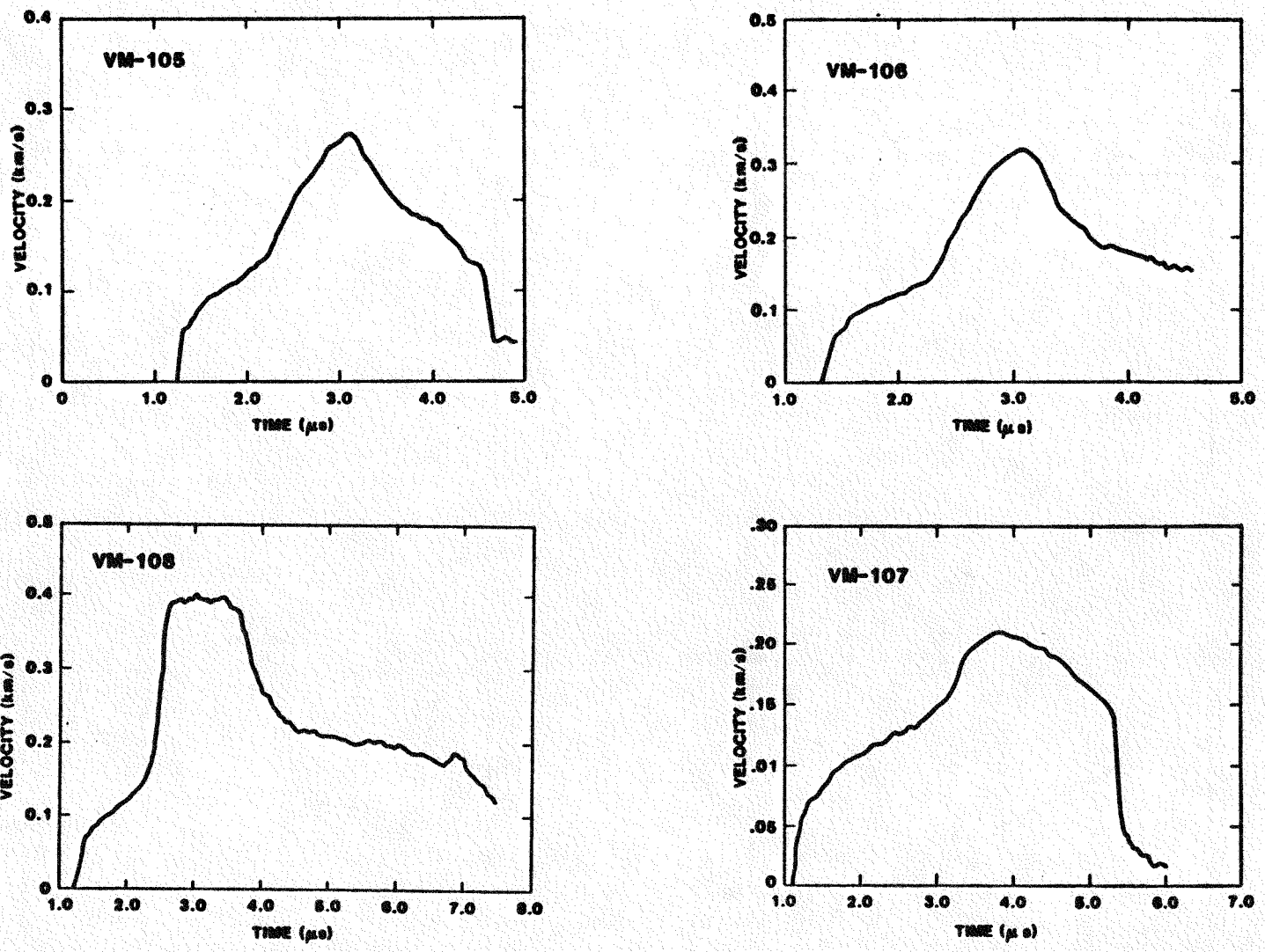

Figure 2. Particle velocity profiles in Vermont marble.

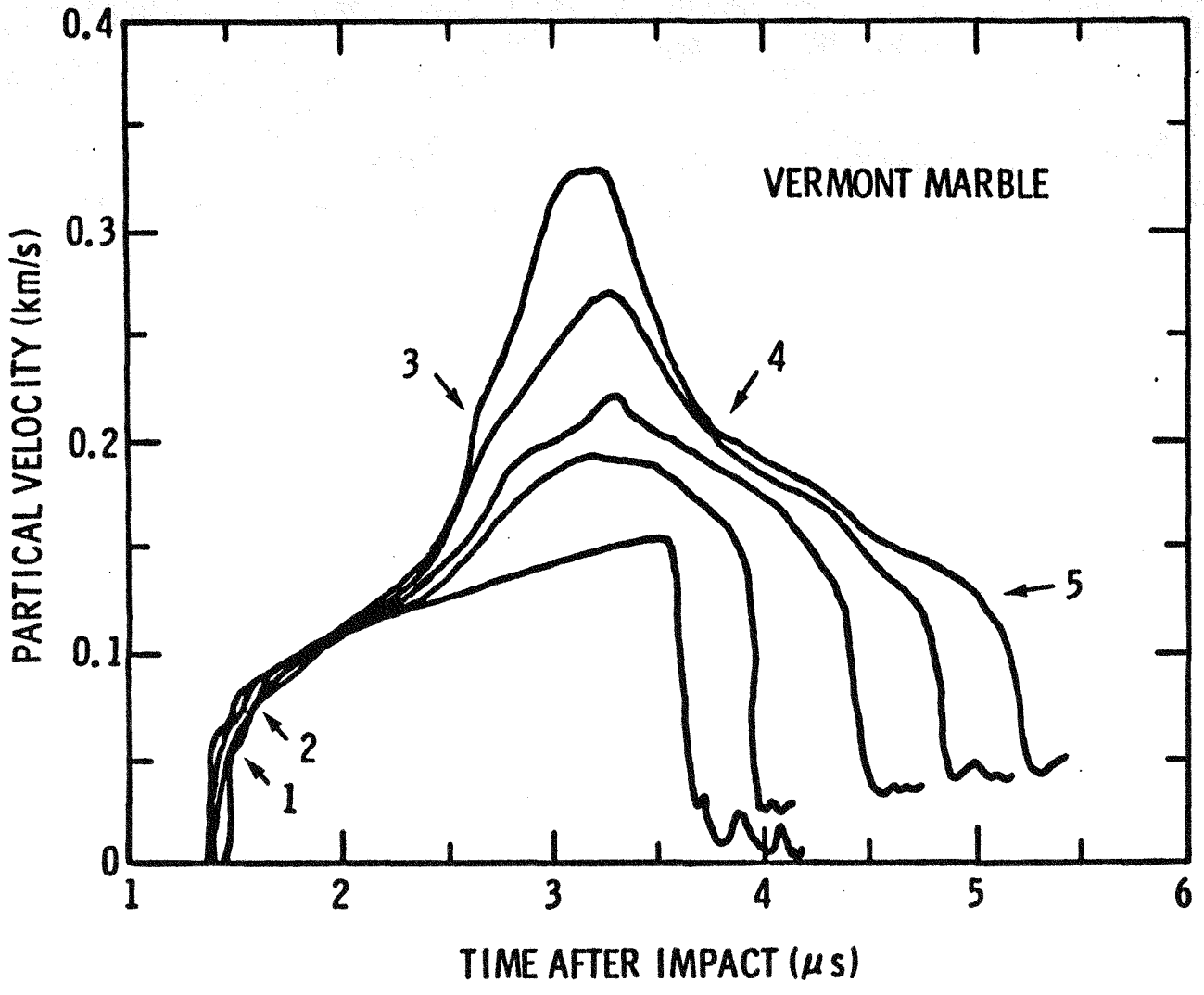

Figure 3. Wave profiles in Vermont marble. The points identified are presumed to be, (1) onset of plastic yielding, (2) onset of calcite I-II phase transformation, (3) onset of calcite II-III phase transformation, (4) initiation of the reverse calcite II-III transformation and, (5) reversion of the calcite I-II transformation through a rarefaction shock wave.

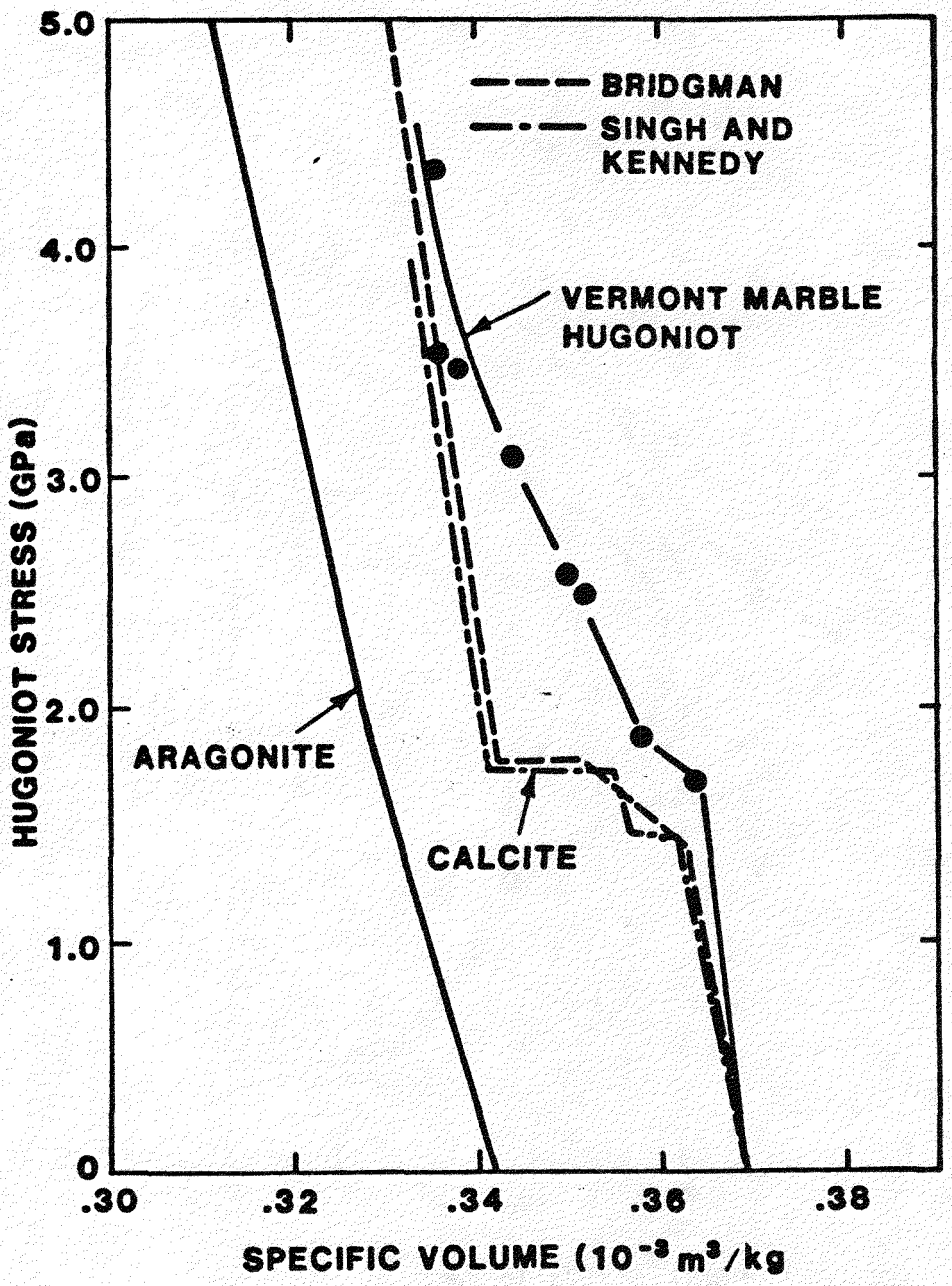

Figure 4. Hugoniot points for Vermont marble through the calcite I-II and calcite II-III phase transition. Comparison is made with hydrostatic isotherms for calcite and aragonite.

3 Stress Relaxation Experiment in Blair Dolomite

A number of competent crustal rocks have demonstrated substantial rate dependence in their strength properties. These effects have been observed in Hopkinson bar experiments and in comparison of shock and static compression response. Blair Dolomite is a rock which has been shown to yield at approximately 0.2 GPa axial stress under static uniaxial-strain loading[7] while stresses in excess of 2.5 GPa before yielding can be supported over the brief duration of a shock wave experiment[8]. Static compression is performed at strain rates of approximately 10^{-4}/s in contrast to shock wave compression which corresponds to a strain rate near 10^{6}/s.

Further experiments were performed on Blair dolomite to investigate rate-dependent strength behavior[9]. In these tests a fused silica ramp-wave generator was used to reduce the risetime of the stress wave before it was coupled into the dolomite sample. Loading rates to nearly 4.0 GPa in the dolomite were achieved at a strain rate of 3×10^{4}/s, nearly two decades lower than the shock-loading experiments. Both the shock- and ramp-wave compression curves are compared with the static uniaxial-strain curve in Figure 5. The ramp-wave compression shows no indication of relaxing toward the static response.

To explore further the question of rate-dependent strength in dolomite a third type of stress-wave experiment has been performed and is described here. This stress-relaxation experiment achieves effective strain-rate response significantly lower than the ramp-wave technique.

3.1 Experimental Method

The experimental configuration used in the present experiment is illustrated in Figure 6 and experimental parameters are provided in Table II. In this experiment a thick dolomite sample is mounted in the projectile and impacted on fused silica. The impact velocity was selected to achieve a stress of approximately 2.0 GPa at the impact interface. The particle velocity was actually measured at a diffusely silvered interface several millimeters from the impact surface to avoid measurement problems due to local surface effects. Approximately 6 μs of uniaxial strain recording is expected before lateral relief waves influence the data.

If the impact stress in the dolomite is maintained and stress relaxation does not occur, then a particle velocity level, constant in time is expected. If stress relaxation occurs in the dolomite within the recording time interval then a corresponding reduction in the measured particle velocity is expected.

Table II
Experimental Parameters for Stress Relaxation Experiments on Blair Dolomite

Shot #	Dolomite Thickness (mm)	Fused Silica Buffer (mm)	Fused Silica Window (mm)	Impact Velocity (km/s)
DS-122	23.00	2.411	38.15	0.255

Note: Sample, window, and buffer diameters were all 75 mm.

3.2 Experimental Results

The measured particle velocity profile for test DS-122 is shown in Figure 7. A particle velocity of 0.16 km/s is obtained on impact and maintained for approximately 6μs before an abrupt rise, presumably due to lateral relief, occurs, followed shortly by signal cut off from wave arrival at the window back surface. The measured projectile velocity and particle velocity correspond to a particle velocity jump of 0.095 km/s in the dolomite and an axial stress jump of 1.96 GPa. The measured stress-particle velocity point is compared with the shock-wave stress-strain paths from reference 2 in Figure 8. As observed, the present Hugoniot point is in good agreement with the earlier work and there is no indication of stress relaxation over the 6μs recording time.

3.3 Discussion

To assess the sensitivity of the experimental method, we have used the hydrostat for Blair dolomite measured by Heard et al.[7] to establish a hydrostatic stress-particle velocity Hugoniot. Comparison with the shock Hugoniot, for dolomite and fused silica in a stress-particle velocity plot shows that a stress relaxation of 0.45 GPa and a particle velocity reduction of 0.023 km/s is expected if shear relaxation to the hydrostat occurs. This particle velocity level

is compared with the measured particle velocity in an expanded plot in Figure 9, demonstrating that the technique should be readily sensitive to the expected level of stress relaxation.

We conclude that relaxation of strength is not occurring in Blair dolomite within the time duration of the present experiment. Over the interval of 6μs this corresponds to an effective strain rate of approximately 2×10^3/s, nearly a decade lower than the earlier ramp-wave tests.

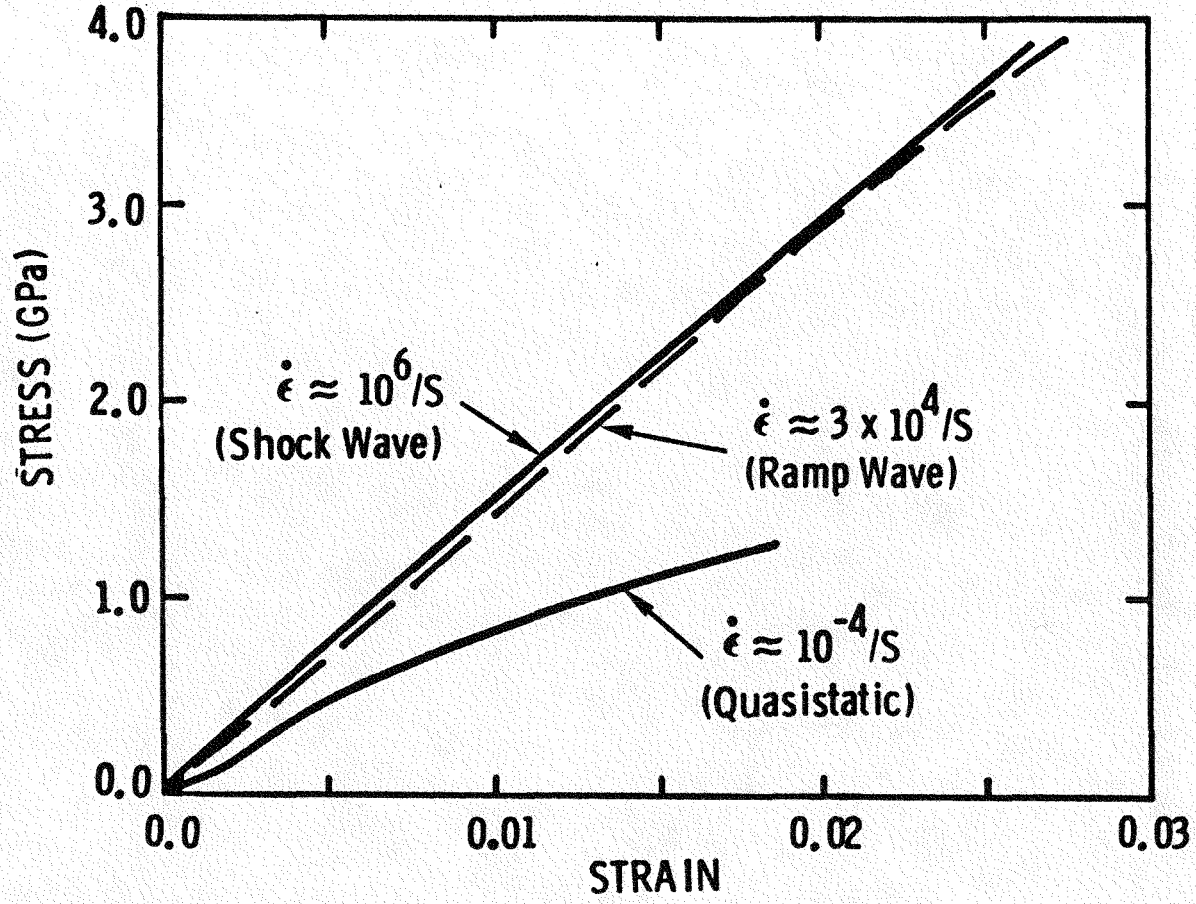

Figure 5. Stress-strain loading paths for Blair dolomite under shock wave, ramp wave, and quasistatic loading rates.

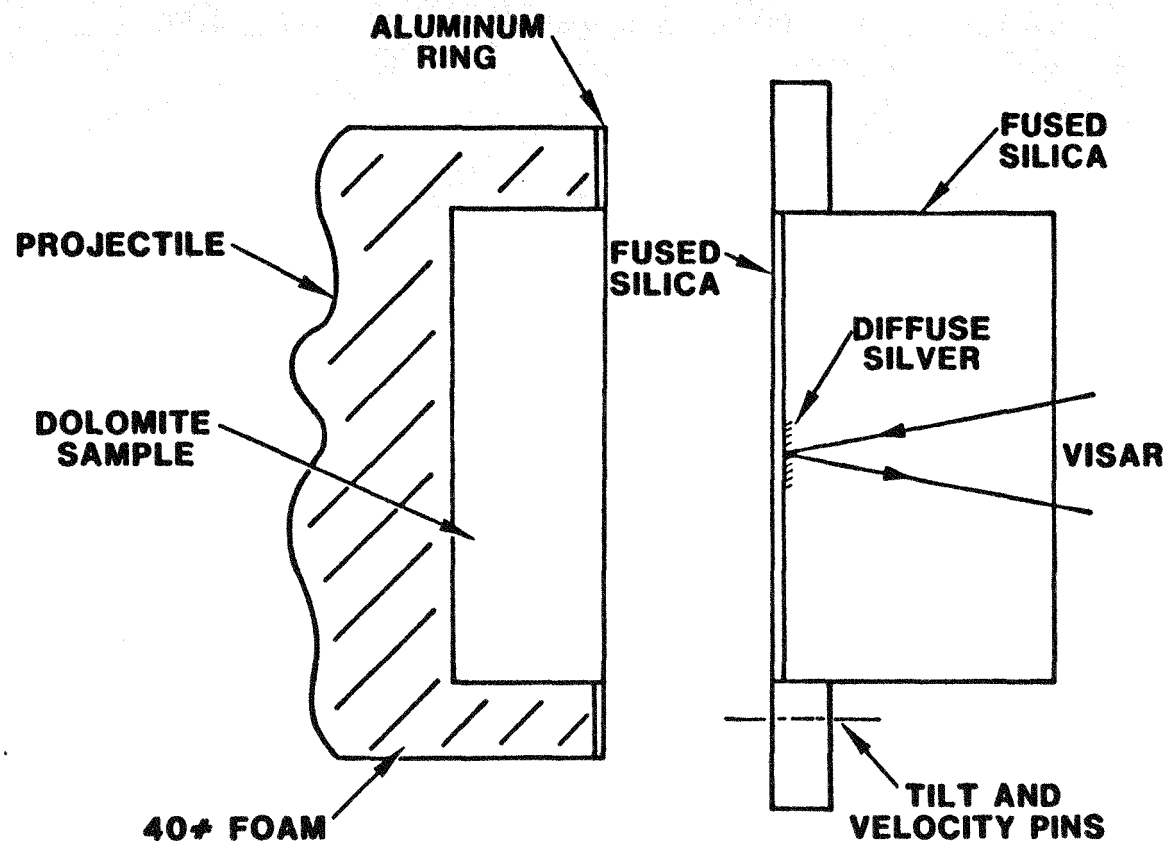

Figure 6. Target and impactor configuration for stress relaxation experiments on Blair dolomite.

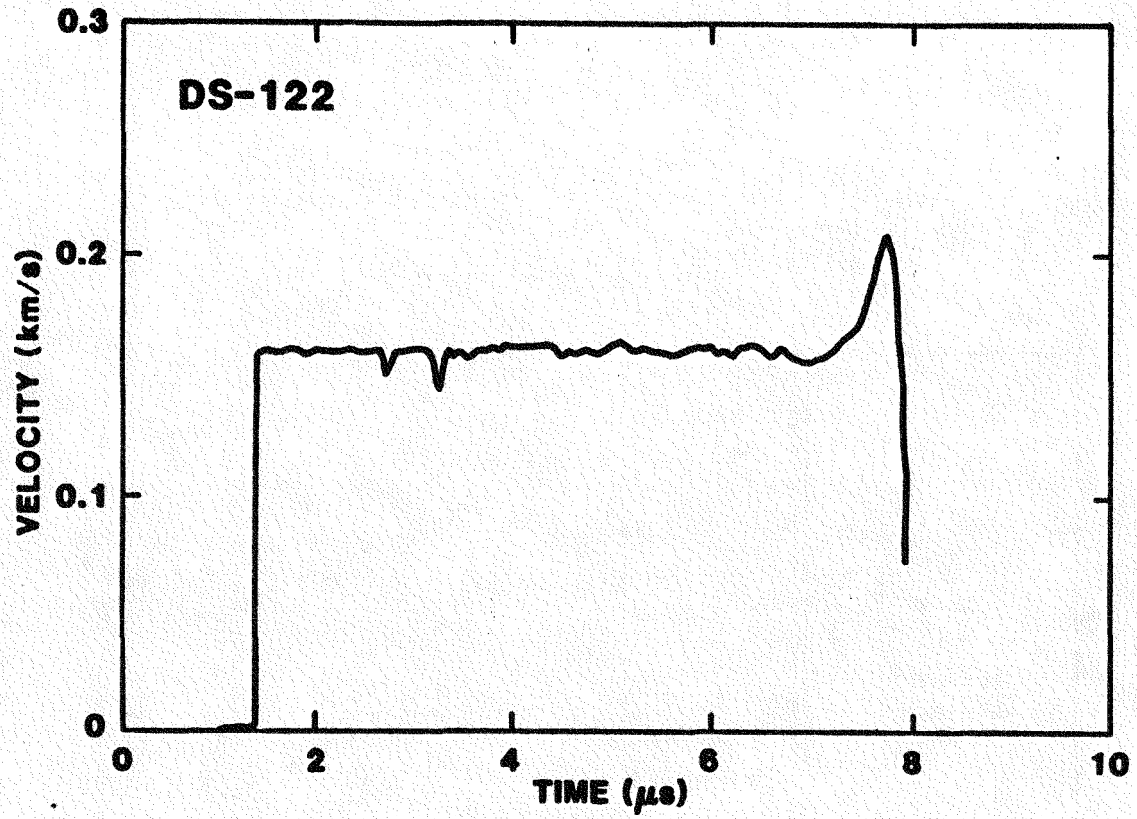

Figure 7. Particle velocity history for stress relaxation experiment in Blair dolomite.

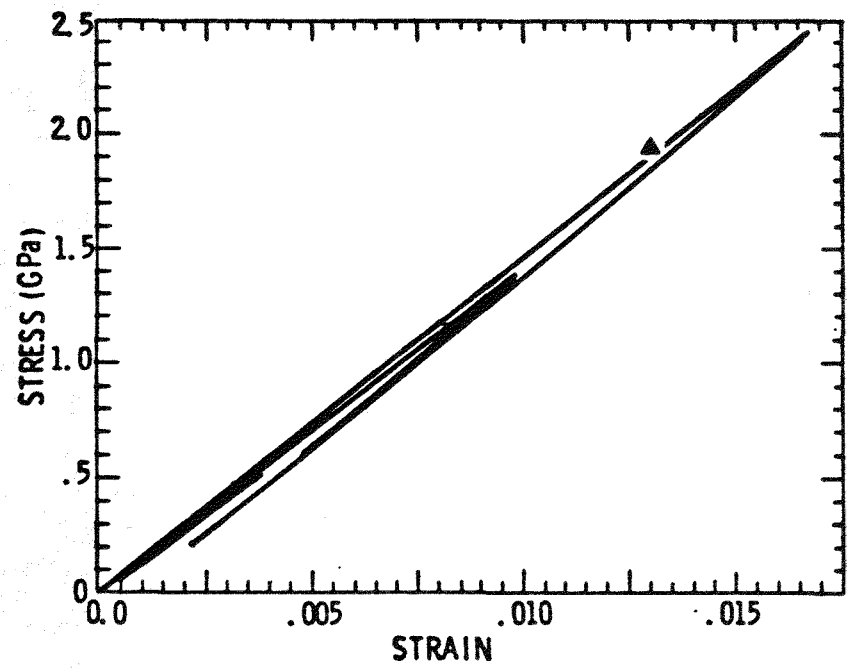

Figure 8. Comparison of measured impact stress level with earlier shock loading paths for Blair dolomite.

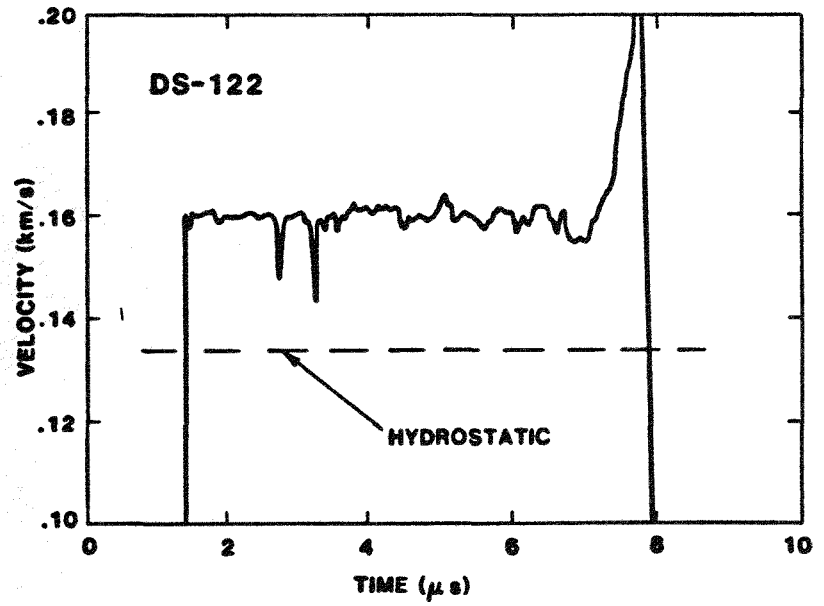

Figure 9. Comparison of expected stress relaxation level with measured particle velocity.

4 Dynamic Dilatancy Experiments in Oakhall Limestone

The occurrence of dilatant void volume in rock due to non-hydrostatic stresses has been found to be a common phenomenon in rock mechanics. It can have significant effect on stress-wave propagation and some effort has been focused on incorporating dilatancy into constitutive models. Dilatancy has not yet been identified in stress-wave experiments, however.

Brace and Riley[10] have conducted static uniaxial-strain experiments on some 15 rocks to 3 GPa and note significant dilatancy in a number of the non- or low-porosity rocks. They note that the largest dilatancy occurs in the calcite rocks (white marble and Oakhall limestone). For instance Oakhall limestone strained in compression to a strain of 0.0175 exhibits a dilatant strain of approximately —0.005 on release or approximately a 30% effect.

Shock loading results in uniaxial-strain loading also and therefore, similar levels of dilatant strain should be observed if the phenomenon is not rate dependent. Two exploratory experiments were undertaken in an attempt to verify dilatancy under shock loading. In these experiments magnetic strain gages, free surface velocity interferometry, and post-shock density measurements were used.

4.1 Experimental Method

The experimental configuration used in the present tests is shown in Figure 10 and the parameters are provided in Table III. In these tests a thick limestone specimen was impacted against a limestone target at velocities near 0.345 km/s which provided a slightly greater peak compressive strain than that achieved in the static experiments of Brace and Riley[10]. The target sample was loaded to approximately 1.5 GPa and then unloaded (also in uniaxial strain) after wave reflection from the back free surface.

4.2 Magnetic Strain Gage Instrumentation

This magnetic technique was developed to measure either in-material particle velocity or strain. Two photoetched copper rings, less than 0.012 mm thickness and 5 mm in diameter are placed concentrically in the sample as shown

in Figure 11. The two rings form a mutual inductor with a mutual inductance M(x) dependent on their separation x. Electrical leads to the two rings exit from the side of the sample and through one ring a pulsed 200 amp current is maintained for the duration of the test. The second "passive" ring is monitored with oscilloscopes.

Table III
Experimental Parameters for Dilatancy Experiments
on Oakhall Limestone

Shot #	Impactor Thickness (mm)	Sample 1 Thickness (mm)	Sample 2 Thickness (mm)	Sample 3 Thickness (mm)	Impact Velocity (km/s)
LS-116	11.97	0.980	0.980	0.968	0.345
LS-117	11.99	0.996	0.985	0.991	0.344

Note: The impactor diameter was 25 mm while the target sample diameters were 35 mm. The diameter difference increased recording time before failure of the ring gage electrical leads.

Due to current I the flux linkage is

$$\phi = MI\,, \tag{1}$$

and the induced EMF is

$$\mathcal{E} = \frac{d\Phi}{dt} = I\frac{dM}{dt} = I\frac{dM}{dx}u\,, \tag{2}$$

where u is the relative velocity between the active and passive ring. The quantity $I\,dM/dx$ provides a "gage factor" between the measured EMF and the in-material particle velocity. In principle, the mutual inductance between concentric rings can be solved exactly in terms of elliptic integrals, but this calibration approach was not pursued. In the present tests it was simpler to relate the known particle velocity associated with the Hugoniot elastic limit observed in the gage record to determine a factor between the measured EMF and particle velocity.

In the present experiments the relative displacement between rings was determined from the EMF records through,

$$\delta x = \int_{t_o}^{t} u dt\,, \tag{3}$$

and the average strain is $\delta x/x_o$ where x_o is the initial ring separation. Records for the two experiments are shown in Figure 12. The positive pulse provides the maximum loading strain while the negative pulse determines the unloading strain. The sign of the final permanent strain is determined by the relative areas of the positive and negative pulses.

From the two records a maximum compressive strain of 0.022 and 0.024 was determined from the positive EMF signal for tests LS-116 and LS-117, respectively. Within the approximately 2% error of the planimeter used to measure the area, the total EMF curve integrated to zero indicating unloading to the same initial strain. If the degree of dilatancy observed by Brace and Riley[10] had occurred, the negative pulse should have had an increased area of approximately 30%.

4.3 VISAR Free Surface Velocity Instrumentation

Velocity interferometry was also used to measure the back free surface velocity during the tests. A 2000Å silver coating was vapor deposited on the back limestone sample to provide a diffusely reflecting surface for the VISAR. The measured free surface velocities for the two experiments are shown in Figure 13.

The particle velocity corresponding to a shock wave emerging at the back surface of the sample can also be used to calculate the final strain. For an elastic material the free surface velocity is exactly twice the in-material particle velocity. If, however, the final strain on unloading is less than (or greater than) zero, the free surface velocity reflects this difference. We have used several methods to estimate the magnitude of the free surface velocity corresponding to a particular dilatant strain level.

To calculate the final free surface velocity the locus of unloading stress and strain states must be known. If only the final dilatant strain value is known, ϵ_f, then a variational method similar to that described by Ahrens et al.[11] can be used to bound, or calculate a corresponding maximum free surface velocity. In terms of the Hugoniot strain, ϵ_h, and particle velocity, u_h, this method provides

$$u_{fS} = 2u_h\left(\frac{1}{2} + \frac{1}{2}\sqrt{1 - \epsilon_f/\epsilon_h}\right). \tag{4}$$

We have assumed a dilatant strain equal to that measured by Brace and Riley[10] on Oakhall limestone which results in the free surface velocity level denoted by 1 in Figure 13.

A further calculation was performed where unloading data for Oakhall limestone[3] was used to estimate a parabolic fit to the locus of stress-strain states with a final state again equal to the dilatant strain observed by Brace and Riley[10]. The Riemann integral was then calculated to determine the free surface velocity. This free surface velocity calculation is denoted by 2 in Figure 13.

Lastly we assumed strain recovery on unloading (no dilatancy) in which case the free surface velocity should equal the projectile velocity, since a symmetric impact of limestone on limestone was performed. This is level 3 in Figure 13. The free surface velocity data show no indication of dilatant strain.

4.4 Post-Test Density Measurements

Nine fragments from the two experiments were recovered and densities were determined with immersion methods by the Sandia standards laboratory. A density of 2696 ± 40 kg/m^3 was determined which is within 0.15% of the initial density. Scatter in the measurement, plus the fact that some of the fragments were probably from the sample periphery, makes this the least definitive test.

4.5 Discussion

The conclusion from the magnetic strain gage, free surface velocity measurements, and post-test density measurements is that dilatant straining is not occurring under dynamic uniaxial strain conditions. This contrasts with the very significant dilatant strain measured by Brace and Riley[10] under conditions of static uniaxial strain, suggesting that dilatant straining is a rate sensitive phenomenon.

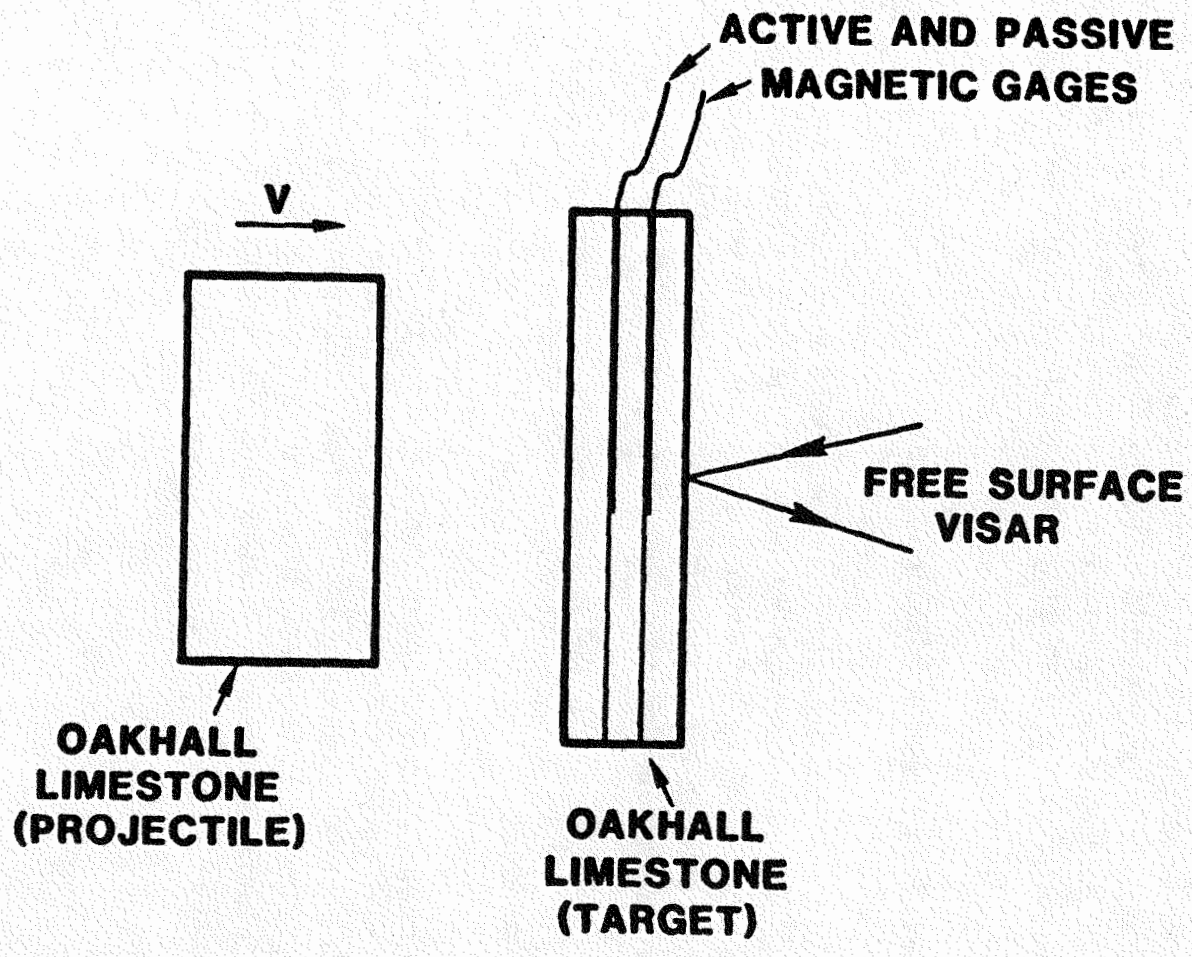

Figure 10. Target and impactor configuration for dynamic dilatancy experiments in Oakhall limestone.

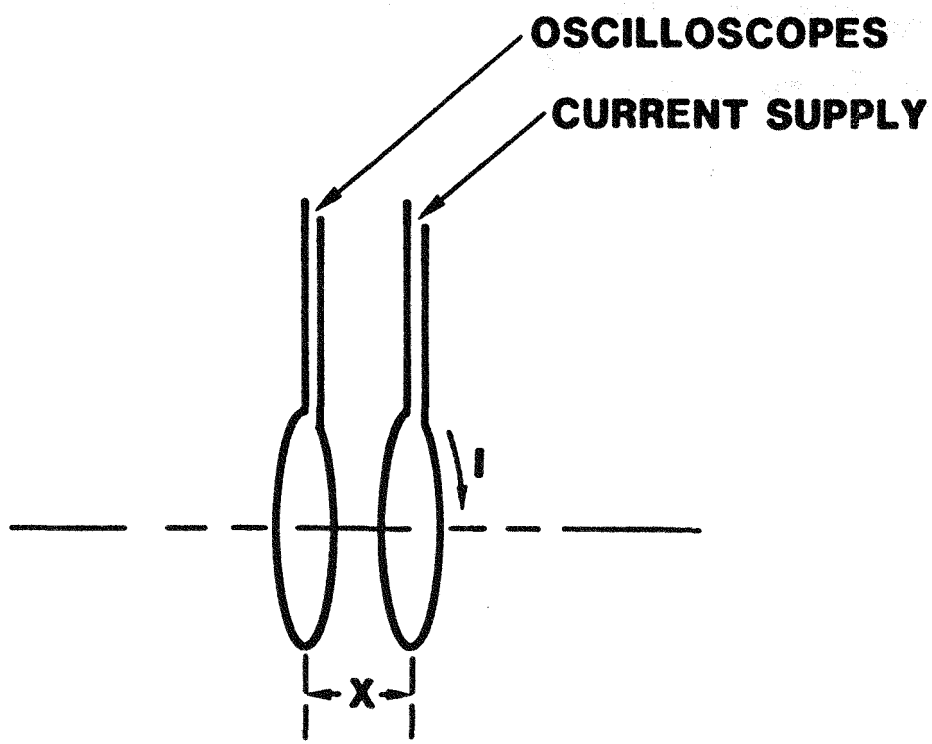

Figure 11. Configuration for mutual inductance particle velocity or strain gage.

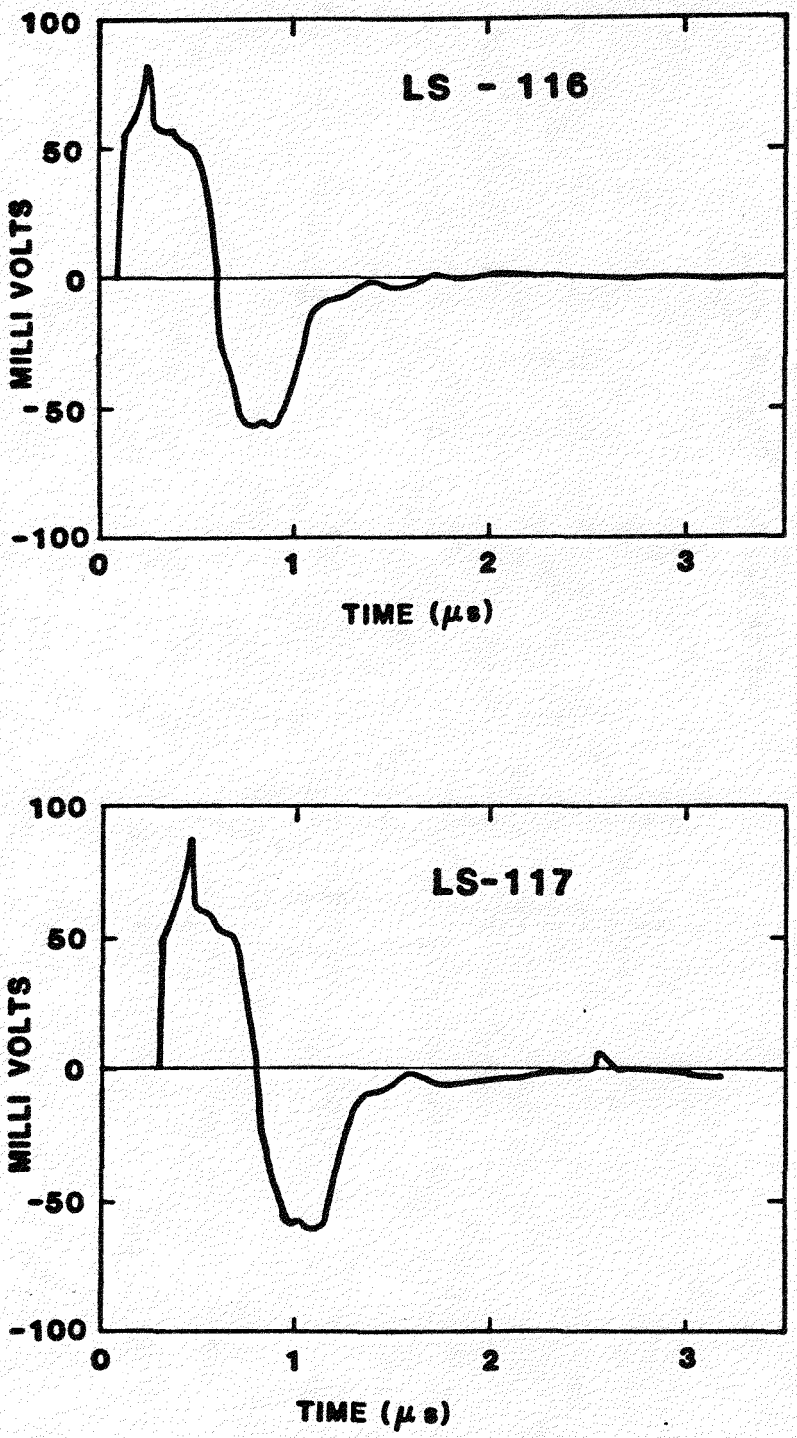

Figure 12. Time-resolved EMF measurements from mutual gages in Oakhall limestone shock and release experiments.

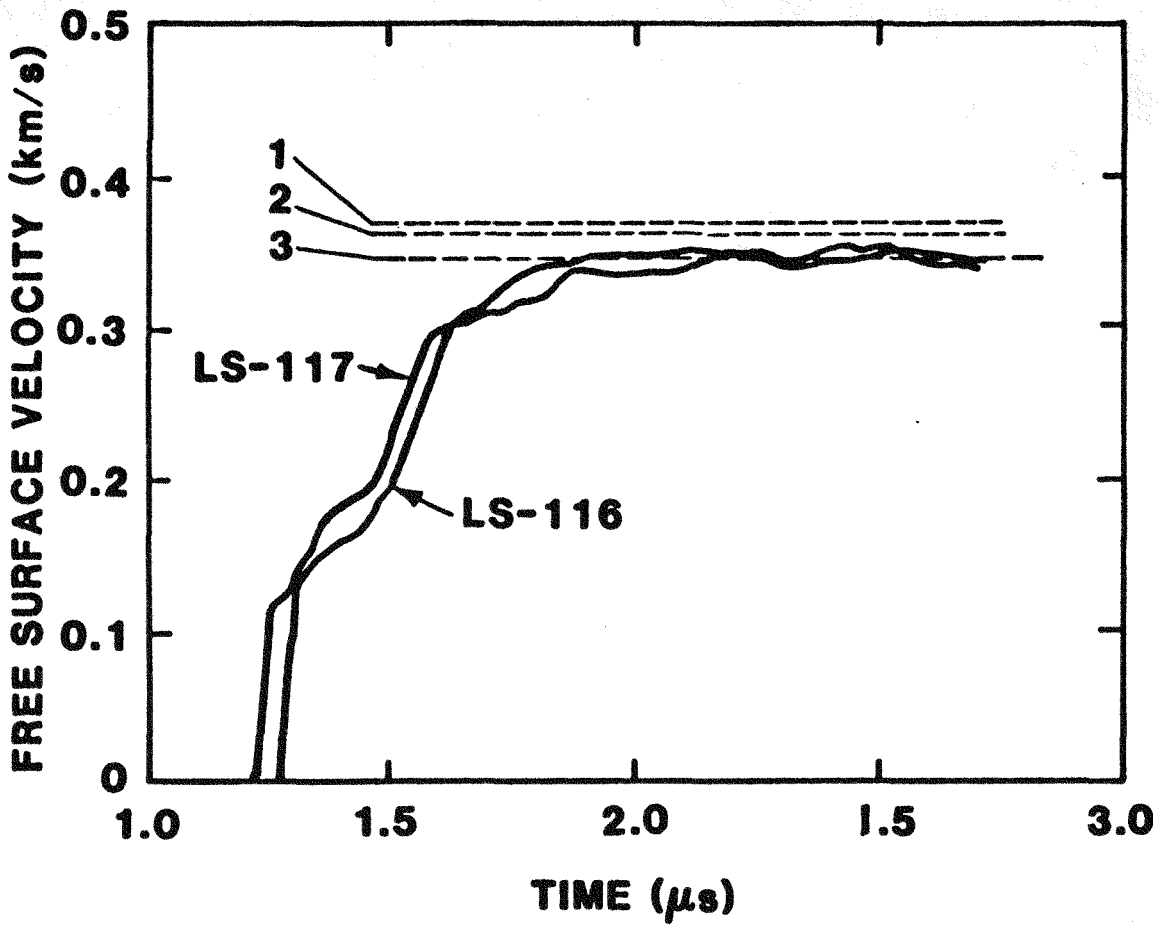

Figure 13. Comparison of free surface motion measurements with calculated values in Oakhall limestone.

5 Stress-Wave Experiments on Single-Crystal Calcite

An extensive study on the compression- and release-wave behavior of calcite rock[4,5] has revealed the complexity of stress-wave propagation in this material. Two physically different phase transformations and plastic yielding play a role in dynamic deformation and both microstructure and shear-stress effects complicate the response. Constitutive modelling of several aspects of the dynamic material behavior has been proposed, however a firmer foundation for constitutive modelling would be available if the wave propagation properties of the component single-crystal material were better understood.

Consequently, an exploratory study of single-crystal calcite was undertaken to qualify response and establish the experimental method. Three loading and release velocity interferometer experiments were completed on z-cut, [0001] calcite over the stress range within which phase transformation and/or yielding was expected.

5.1 Experimental Method

The experimental method selected to study large amplitude wave propagation in calcite was similar to that of earlier studies[4]. A fused silica plate backed by a light carbon foam and carried on a 4 inch diameter gas gun projectile was caused to undergo planar impact on the calcite samples. Experimental conditions are provided in Table IV.

Table IV.
Parameters for Stress-Wave
Experiments on Single-Crystal Calcite

Test #	Orientation	Impactor Thickness (mm)	Sample Thickness (mm)	Buffer Thickness (mm)	Window Thickness (mm)	Impact Velocity (km/s)	First Arrival Velocity (km/s)
CA-101	[0001]	2.383	5.043	0	12.782	0.601	5.75
CA-102	[0001]	2.379	4.958	0	12.785	0.451	5.82
CA-103	[0001]	2.392	5.035	3.016	12.692	0.520	5.68

Large single crystals of Islandic Spar calcite from Chihuahua, Mexico with density of 2710 kg/m^3 were acid saw cut to provide faces normal to the [0001] axis. X-ray crystallography showed that all samples were within 2° of the desired orientation.

Fused silica windows were bonded to the back of the calcite and the motion of the interface was monitored with the diffused velocity interferometer. In one case a fused silica buffer was used. The BRACIS[12], a laser technique for accurately monitoring the time of impact, was used to determine shock velocities. It was found necessary to orient the BRACIS laser light normal to the cleavage plane to avoid the confusion of double beams.

5.2 Experimental Results

The velocity profiles for the three experiments are shown in Figure 14. Tests CA-101 and CA-102 were designed to achieve peak stress amplitudes of approximately 3.5 and 2.5 GPa, respectively. One serious difficulty noted was the high level of noise on the VISAR records in contrast to earlier studies on rocks[1,2,3]. Test CA-103 was performed to attempt to eliminate the noise. The precautions taken included a 3 mm fused silica buffer, significant broadening of the laser spot by defocusing, spike filters on both the BRACIS and VISAR lasers, and total blackening of sample and window. Despite these precautions only modest improvement was noted.

The loading wave profiles shown in Figure 14 for z-cut calcite differ markedly from similar profiles in calcite rock. Sharp loading to 1.84 GPa is noted before yielding by either plastic flow or phase transformation occurs. Two further distinct loading waves are observed. Unloading occurs through an initial dispersive wave followed by a rarefaction shock wave.

5.3 Discussion

The 1.84 GPa amplitude of the first loading wave is in good agreement with Ahrens and Gregson[13], the only other shock-wave study on single-crystal calcite. Whether this break corresponds to plastic yielding or onset of the calcite I-II phase transformation within the elastic response of the calcite is difficult to infer from the limited data. Hydrostatic compression studies on single-crystal calcite identify the calcite I-II transformation at 1.45 GPa and the calcite II-III transition at 1.74 GPa. The approximately 0.2 GPa amplitude of the second loading wave

is consistent with the limited stress range for stability of calcite II observed statically, however. That the shock transformation initiates approximately 0.4 GPa higher and undergoes only about a third of the transformation strain expected statically is not inconsistent with the shear-sensitive, displacive calcite I-II transformation.

Final Hugoniot points are identified with equilibrium hydrostatic compression behavior in Figure 15. As has been observed in earlier studies on calcite rock, transformation toward the calcite III state appears to be occurring within the third loading wave. The final loading states appear to fall on a metastable Hugoniot, however. This behavior is analogous to the character of shock-induced reconstructive transformations observed in silicates. That the calcite Hugoniot in Figure 15 is metastable and not an equilibrium Hugoniot is strengthened by the behavior of the relief waves in Figure 15. Although we have not attempted to determine release stress-strain paths, the slope of the measured Hugoniot is too shallow to be consistent with the initial dispersive release wave followed by a rarefaction shock wave.

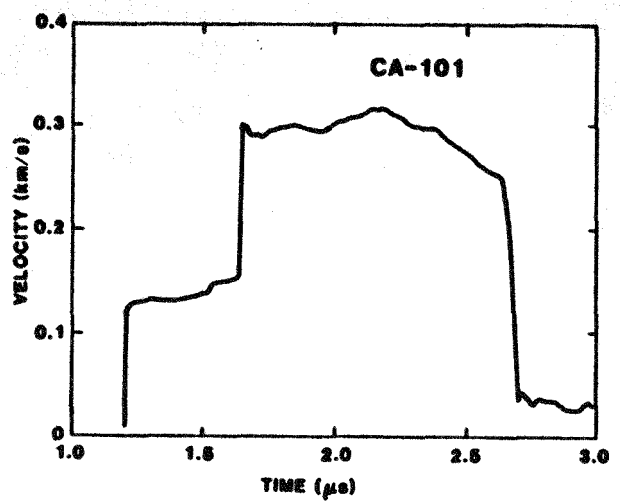

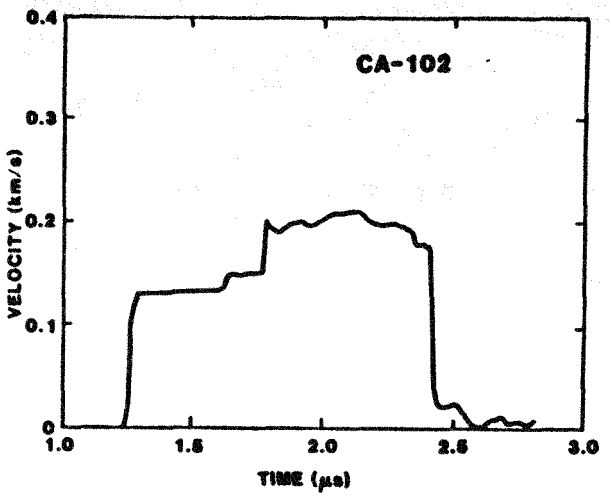

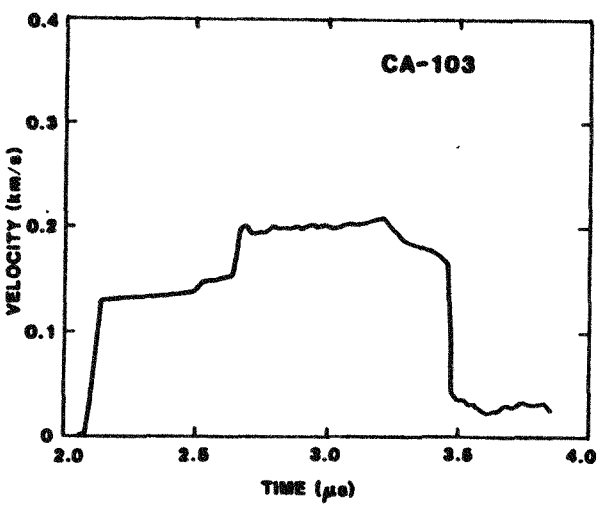

Figure 14. Particle velocity profiles in Z-cut calcite.

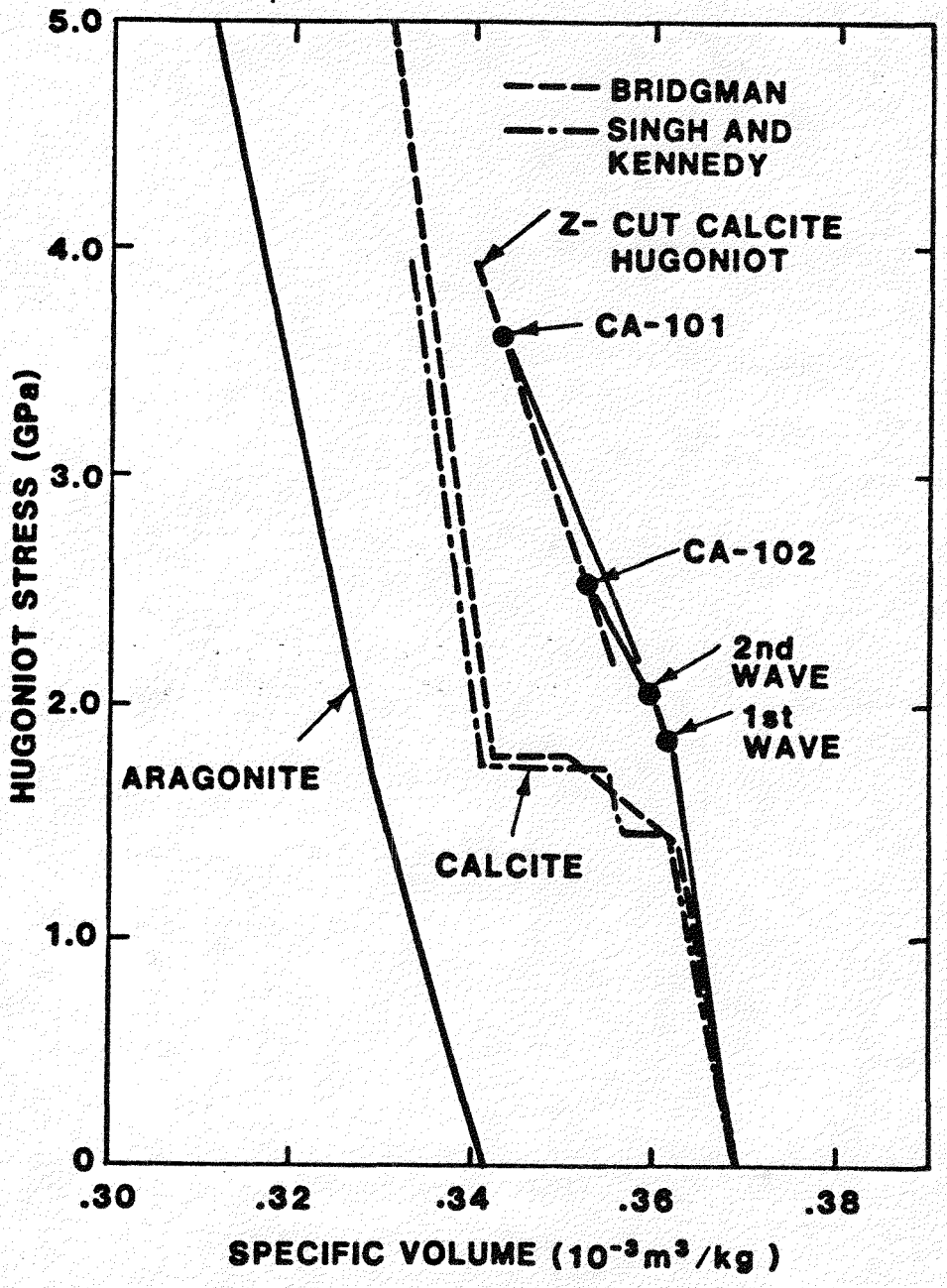

Figure 15. Comparison of Z-cut calcite Hugoniot points with hydrostatic isotherms for calcite and aragonite.

6 Energy Attenuation in Below-Yield Wave Propagation in Oil Shale.

Shock wave studies on oil shale have shown that this material has a nominal Hugoniot elastic limit of 0.2 GPa[14] and subsequent two-dimensional calculations of explosive fracturing have treated oil shale as elastic-plastic with a 0.2 GPa elastic limit[15,16]. Attenuation of wave energy from the head of the wave below the elastic limit of the material can occur by several mechanisms. First, if the material is viscoelastic, real dissipation can occur within the compressive wave. Secondly, if the material is geometrically dispersive, energy can be effectively lost from the head of the pulse due to the different wave velocities associated with different frequency components. Either case is important to modelling oil shale for explosive fracturing calculations in that the energy within the stress wave front is responsible for the initial "shock" fracture and fragmentation of the medium.

To investigate energy dissipation and dispersion in oil shale, a series of wave attenuation experiments were performed at impact levels below the elastic limit of the material. The data were then interpreted in terms of an energy attenuation coefficient.

6.1 Experimental Method

The wave attenuation experiments were performed with a test configuration similar to that described in reference 1. PMMA plates of 2 mm thickness backed by light carbon foam were mounted in a 4 inch diameter gas-gun projectile and caused to impact samples of oil shale. The oil shale samples ranged from 5 to 35 mm in thickness to provide a range of attenuation distances. The sample was backed with a 2 mm PMMA buffer followed by a 25 mm PMMA laser window. The motion of a vapor-deposited mirror was monitored with a Michelson displacement interferometer[17]. The latter was used rather than the VISAR system due to the very low impact velocities required to remain below the elastic limit of the oil shale.

The oil shale studied was 80 mℓ/kg kerogen content carbonate marlstone obtained from the Anvil Points mine near Rifle, Colorado. The material has a density of 2150 kg/m^3 and an elastic wave speed of 3.0 km/s. Samples were oriented so that wave propagation was perpendicular to the planes of bedding.

Impact velocities were selected so that initial stresses of approximately 0.1 and 0.15 GPa were achieved which were well below the Hugoniot elastic limit.

Table V.
Experimental Parameters for Energy Attenuation Experiments in Oil Shale

Test #	Impactor Thickness (mm)	Sample Thickness (mm)	Buffer Thickness (mm)	Impact Velocity (m/s)	Wave Energy kJ/m^2)
OA-102	2.00	5.00	1.96	69.0	4.3
OA-103	2.01	14.76	2.05	70.8	3.9
OA-105	2.01	25.00	1.71	70.0	2.9
OA-106	2.01	34.96	1.74	67.4	3.3
OA-108	2.02	35.00	1.75	70.7	2.7
OA-109	2.04	15.98	1.96	47.0	1.8
OA-111	2.00	35.54	1.65	44.7	0.5
OA-114	2.02	23.64	2.20	46.4	1.5

6.2 Experimental Results and Analysis

The experimental conditions for eight low velocity impact experiments are provided in Table V. In Figure 16 measured particle velocity profiles are shown which are time correlated with respect to wave transit across the sample thickness to indicate the magnitude of attenuation of the peak particle velocity. In Figure 17 the profiles are displayed in coincidence to better illustrate the extent of wave dispersion. Over the approximately 30 mm sample thickness, wave propagation in oil shale is not elastic but shows a statistically significant attenuation of the peak stress and dispersion in the wave profile shape.

To provide a measure of the energy in the stress pulse we will use the expression,

$$E = \int_o^{t_p} \sigma u dt , \tag{5}$$

where the product of the stress and particle velocity, σu, is the rate of work per unit area by the pulse on an in-material plane of oil shale. Integration over the total duration of the stress pulse provides the wave energy at that propagation distance. The measured particle velocity profiles are the transmitted profiles at

the oil shale – PMMA interface which represents a fairly significant impedance mismatch. To provide a measure of the in-material oil shale profile incident on the interface the experimental profile was multiplied by the factor $(Z_p + Z_o)/2Z_o$ where Z_p and Z_o are the elastic impedance of PMMA and oil shale, respectively. Values of $Z_p = 3.30 \times 10^6$ and $Z_o = 6.77 \times 10^6$ kg/m^{2}s were used where the latter was determined from a nominal measured wave velocity of 3.15 km/s. The calculated wave energies for the different propagation distances are provided in Table V and compared in Figure 18.

6.3 Discussion

A semilog plot of the wave energy attenuation data is provided in Figure 18. One data point for the lower amplitude data is off the plot and has been ignored. The results are reasonably well described by $E = E_o e^{-x/x_o}$ where E_o is the input stress-wave energy. For the present oil shale experiments we find that the wave energy attenuates to $1/e$ of its initial value in a propagation distance of 56 mm. This is a significant discrepancy from the currently assumed linear elastic response within this stress range.

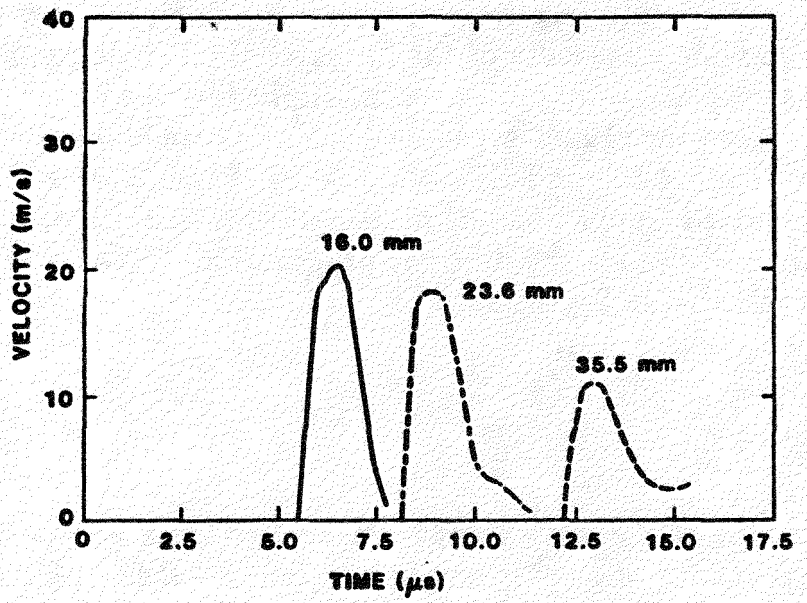

(a). Nominal 0.1 GPa impact stress amplitude.

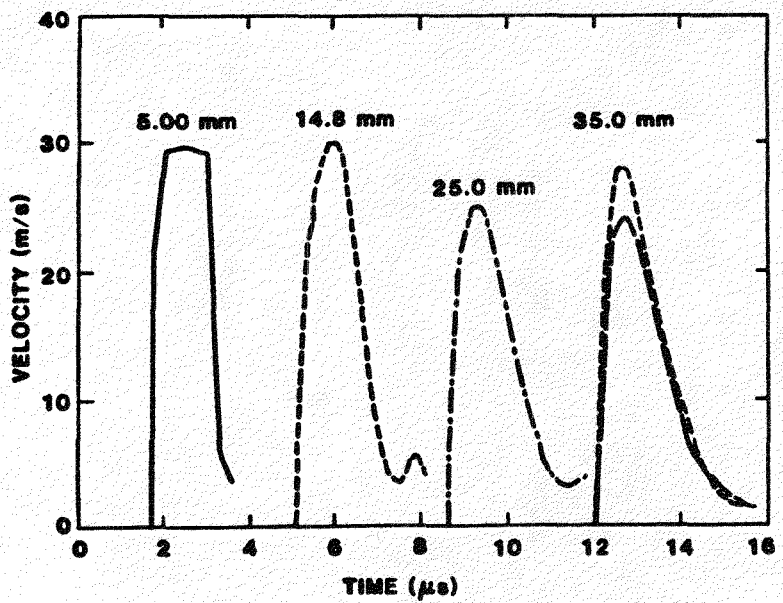

(b). Nominal 0.5 GPa impact stress amplitude.

Figure 16. Time correlated particle velocity profiles in oil shale for wave attenuation experiments.

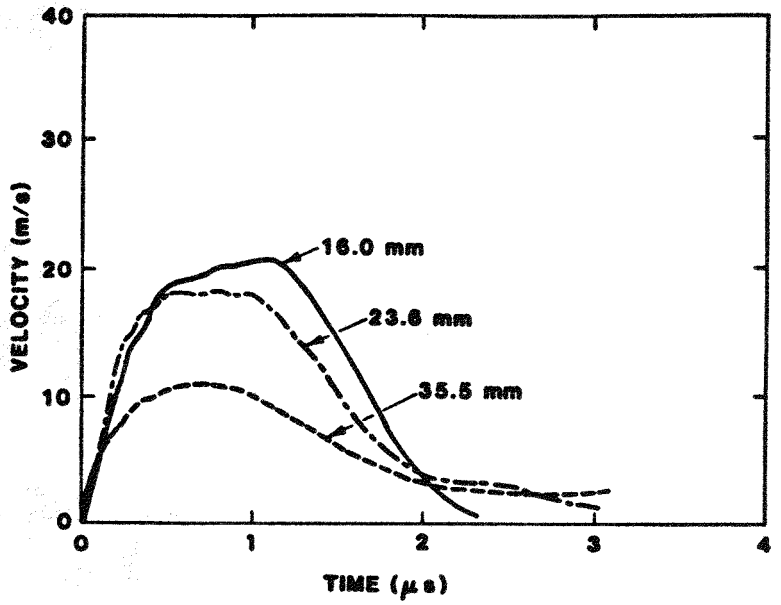

(a). Nominal 0.1 GPa impact stress amplitude.

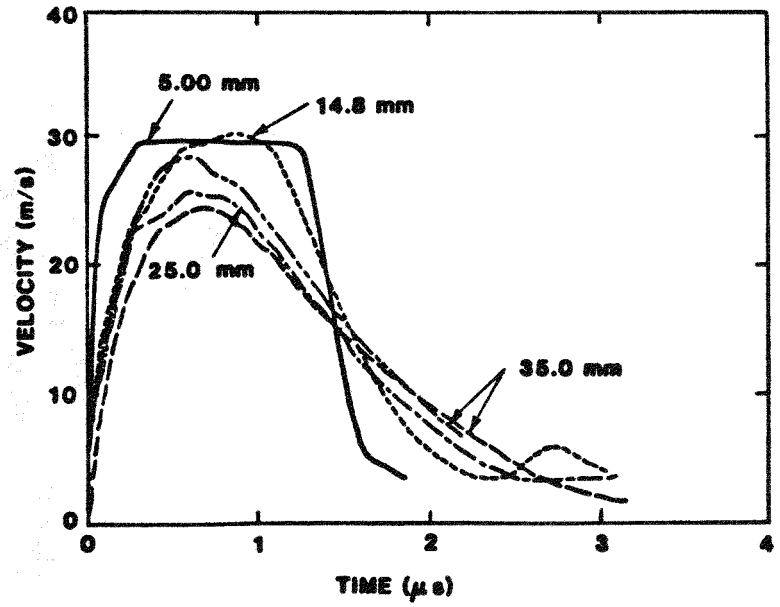

(b). Nominal 0.15 GPa impact stress amplitude.

Figure 17. Coincident particle velocity profiles in oil shale for wave attenuation experiments.

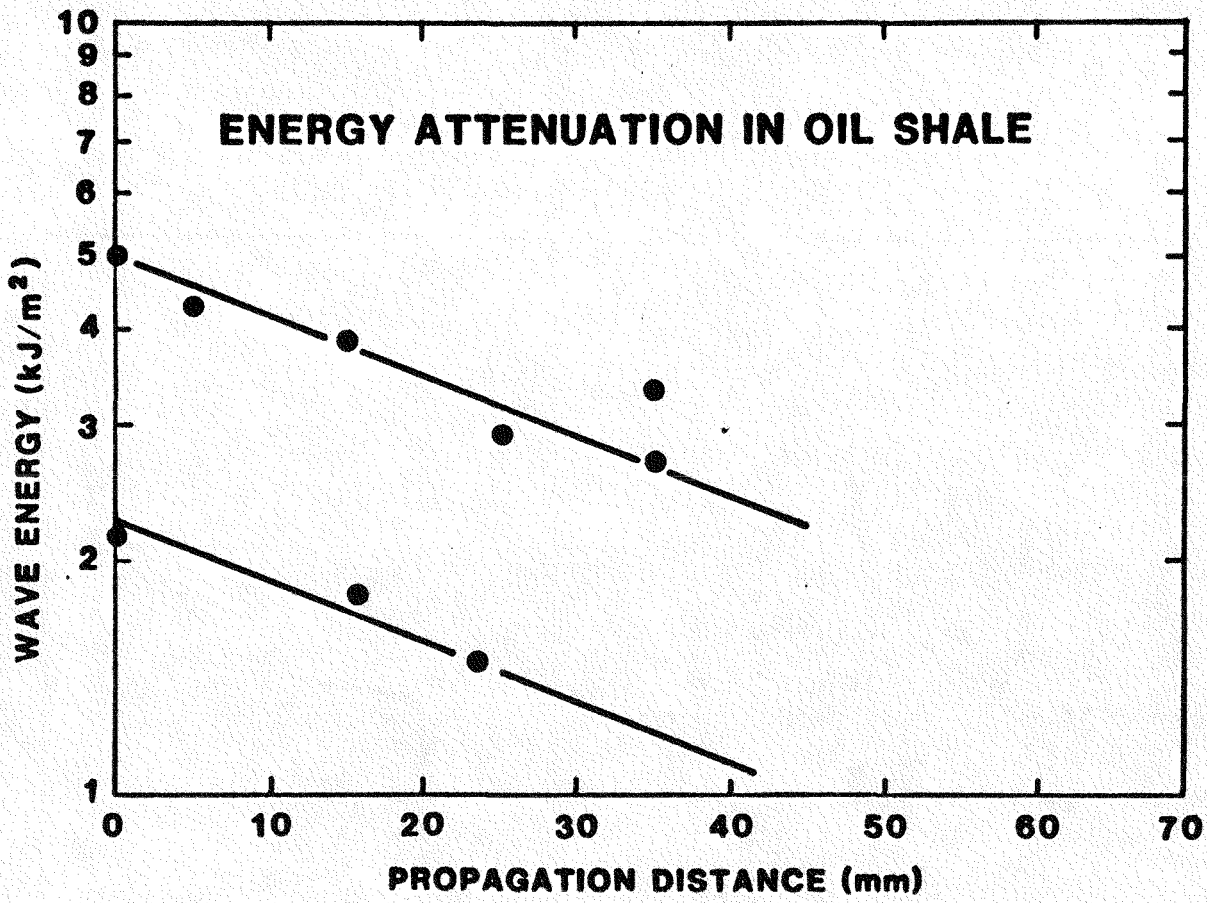

Figure 18. Energy attenuation with propagation distance in oil shale.

7 Closure

Several experimental studies on various crustal rocks and minerals have been described which were conducted to explore specific details in response to compressive stress-wave loading. One new experimental method has also been described while variations and specific difficulties with previous techniques have been documented. Simple wave experiments on Vermont marble show yielding by plastic flow followed immediately by onset of displacive phase transformation. Impact experiments on Blair dolomite fail to show stress relaxation to measured quasistatic uniaxial stress-strain response. Compressive loading and unloading wave experiments do not indicate dilatant strain under uniaxial strain loading conditions in Oakhall limestone. Preliminary experiments on Z-cut calcite show multiple wave structure associated with plastic yielding and phase transformation. Lastly, wave attenuation experiments on oil shale show significant energy dissipation or dispersion at stress levels below the measured Hugoniot elastic limit.

8 Acknowledgements

The efforts of R. E. Hollenbach in performing a large number of the experiments are deeply appreciated.

References

[1] **D. E. Grady, R. E. Hollenbach, K. W. Schuler, and J. F. Callender**
Compression Wave Studies in Blair Dolomite,SAND76-0005, Sandia National Laboratories, Albuquerque, NM (February, 1976).

[2] **K. W. Schuler and D. E. Grady**
Compression Wave Studies in Solenhofen Limestone, SAND76-0279, Sandia National Laboratories, Albuquerque, NM (May, 1977).

[3] **D. E. Grady**
Compression Wave Studies in Oakhall Limestone, SAND83-0370, Sandia National Laboratories, Albuquerque, NM (March, 1983).

[4] **D. E. Grady, R. E. Hollenbach, and K. W. Schuler**
Compression Wave Studies on Calcite Rock,*J. Geophys. Res.* **83**, 2839-2848, 1978.

[5] **D. E. Grady**
Interrelation of Flow or Fracture and Phase Transition in the Deformation of Carbonate Rock, *J. Geophys. Res.* **84**, 7549-7554, 1979.

[6] **D. E. Grady**
Coherent Phase Transformation Under Nonhydrostatic Stress Wave Loading, *J. Geophys. Res.* (submitted).

[7] **H. C. Heard, A. Duba, A. E. Abey, and R. N. Shock**
Mechanical Properties of Blair Dolomite, UCRL-51465, Lawrence Livermore National Laboratories, Livermore, CA 1973.

[8] **D. E. Grady, R. E. Hollenbach, K. W. Schuler, and J. F. Callender**
Strain Rate Dependence on Dolomite Inferred from Impact and Static Compression Studies, *J. Geophys. Res.* **82**, 1325-1333, 1977.

[9] **D. E. Grady**
High Strain Rate Studies in Rock, *Geophys. Res. Lett.* **1**, 263-266, 1977.

[10] **W. F. Brace and D. K. Riley**
Static Uniaxial Deformation of 15 Rocks to 30 kb, *Int. J. Rock. Mech. Min. Sci.* **9**, 271-288, 1972.

[11] **T. J. Ahrens, J. T. Rosenberg, and M. H. Rosenberg**
Dynamic Properties of Rock, Stanford Research Inst. Rept. DASSA 1868, Menlo Park, CA 1966.

[12] **L. M. Barker and R. E. Hollenbach**
Shock Wave Studies of PMMA, Fused Silica and Sapphire, *J. Appl. Phys.* **41**, 4208-4226, 1970.

[13] **T. J. Ahrens and V. G. Gregson**
Shock Compression of Crustal Rocks: Data for Quartz, Calcite and Plagioclase Rocks, *J. Geophys. Res.* **69**, 4839-4874, 1964.

[14] **D. E. Munson**
In Situ Oil Shale Bed Preparation Study: Progress Rept., Feb. 1976 to Feb. 1978, SAND78-1950, Sandia National Laboratories, Albuquerque, NM (November, 1978).

[15] **D. E. Grady and M. E. Kipp**
Continuum Modelling of Explosive Fracture in Oil Shale, *Int. J. Rock Mech. Min. Sci.* **17**, 147-157, 1980.

[16] **R. R. Boade, M. E. Kipp, and D. E. Grady**
A Blasting Concept for Preparing Vertical Modified in situ Oil Shale Retorts, SAND81-1255, Sandia National Laboratories, Albuquerque, NM, (December, 1981).

[17] **L. M. Barker and R. E. Hollenbach**
Interferometer Technique for Measuring Dynamic Mechanical Properties of Materials, *Rev. Sci. Inst.* **36**, 1617, 1965.

DISTRIBUTION:

C. K. B. Lee
R& D Associates
P. O. Box 9695
Marina Del Rey, CA 90291

T. J. Ahrens
California Institute of Technology
Pasadena, CA 91109

D. R. Curran
Stanford Research Institute
333 Ravenswood Avenue
Menlo Park, CA 94025

Y. M. Gupta
Department of Physics
Washington State University
Pullman, WA 99163

H. C. Heard
Lawrence Livermore Laboratory
P. O. Box 808
Livermore, CA 94550

C. Petersen
Systems, Science & Software
P. O. Box 1620
La Jolla, CA 92038

L. G. Margolin
Los Alamos National Laboratory
Los Alamos, NM 87545

R. J. Clifton
Department of Engineering
Brown University
Providence, RI 02912

R. Jeanloz
Dept. of Geology and Geophysics
University of California
Berkeley, CA 94720

D. P. Dandekar
Army Materials and Mechanics
Research Center
Watertown, MA

Sandia Internal:

1500 W. Herrmann
1510 D. B. Hayes
1520 T. B. Lane
1522 K. W. Schuler
1530 L. W. Davison
1531 B. J. Thorne
1533 P. Yarrington
1533 T. K. Bergstresser
1533 M. E. Kipp
1533 J. W. Swegle
1534 J. R. Asay
1534 L. M. Barker
1534 L. Chhabildas
1534 D. S. Drumheller
1534 D. E. Grady (25)
1534 T. G. Trucano
1534 J. L. Wise
1540 W. C. Luth
1542 B. M. Butcher
1542 L. S. Costin
8214 M. A. Pound
3141 L. J. Erickson (5)
3151 W. L. Garner (3)
3154-4 C. Dalin (25)
FOR DOE/TIC